

Pre-plasma effect on energy transfer from laser beam to shock wave generated in solid target

T. Pisarczyk, S. Yu. Gus'kov, Z. Kalinowska, J. Badziak, D. Batani, L. Antonelli, G. Folpini, Y. Maheut, F. Baffigi, S. Borodziuk, T. Chodukowski, G. Cristoforetti, N. N. Demchenko, L. A. Gizzi, A. Kaspercuk, P. Koester, E. Krousny, L. Labate, P. Parys, M. Pfeifer, O. Renner, M. Smid, M. Rosinski, J. Skala, R. Dudzak, J. Ullschmied, and P. Pisarczyk

Citation: *Physics of Plasmas* (1994-present) **21**, 012708 (2014); doi: 10.1063/1.4862784

View online: <http://dx.doi.org/10.1063/1.4862784>

View Table of Contents: <http://scitation.aip.org/content/aip/journal/pop/21/1?ver=pdfcov>

Published by the [AIP Publishing](#)

Articles you may be interested in

[The Influence of spot size on the expansion dynamics of nanosecond-laser-produced copper plasmas in atmosphere](#)

J. Appl. Phys. **113**, 243304 (2013); 10.1063/1.4812580

[Dense plasma heating and Gbar shock formation by a high intensity flux of energetic electrons](#)

Phys. Plasmas **20**, 062705 (2013); 10.1063/1.4811473

[Collisionless shock generation in high-speed counterstreaming plasma flows by a high-power laser](#)


Phys. Plasmas **17**, 122702 (2010); 10.1063/1.3524269


[Al 1 s - 2 p absorption spectroscopy of shock-wave heating and compression in laser-driven planar foil](#)

Phys. Plasmas **16**, 052702 (2009); 10.1063/1.3121217


[Laser absorption, mass ablation rate, and shock heating in direct-drive inertial confinement fusion](#)

Phys. Plasmas **14**, 056305 (2007); 10.1063/1.2671690

A collection of five pieces of Pfeiffer Vacuum equipment, including a red turbopump, a silver turbopump, a silver backing pump, a red turbopump with a long shaft, and a silver chamber component.

 Vacuum Solutions from a Single Source

- Turbopumps
- Backing pumps
- Leak detectors
- Measurement and analysis equipment
- Chambers and components

PFEIFFER  **VACUUM**

Pre-plasma effect on energy transfer from laser beam to shock wave generated in solid target

T. Pisarczyk,¹ S. Yu. Gus'kov,² Z. Kalinowska,¹ J. Badziak,¹ D. Batani,³ L. Antonelli,³ G. Folpini,³ Y. Maheut,³ F. Baffigi,⁴ S. Borodziuk,¹ T. Chodukowski,¹ G. Cristoforetti,⁴ N. N. Demchenko,² L. A. Gizzi,⁴ A. Kasperczuk,¹ P. Koester,⁴ E. Krousky,⁵ L. Labate,⁴ P. Parys,¹ M. Pfeifer,⁵ O. Renner,⁶ M. Smid,⁶ M. Rosinski,¹ J. Skala,⁵ R. Dudzak,⁵ J. Ullschmied,⁵ and P. Pisarczyk⁷

¹*Institute of Plasma Physics and Laser Microfusion, Warsaw, Poland*

²*P.N. Lebedev Physical Institute of RAS, 53 Leninsky Ave., 119 991 Moscow, Russia*

³*Université Bordeaux, CNRS, CEA, CELIA (Centre Lasers Intenses et Applications), UMR 5107, Talence, France*

⁴*Intense Laser Irradiation Laboratory at INO-CNR, Pisa, Italy*

⁵*Institute of Plasma Physics ASCR, v.v.i., Za Slovankou 3, 182 00 Prague 8, Czech Republic*

⁶*Institute of Physics ASCR, v.v.i., Na Slovance 2, 182 21 Prague 8, Czech Republic*

⁷*Warsaw University of Technology, ICS, 15/19 Nowowiejska St., 00-665 Warsaw, Poland*

(Received 17 October 2013; accepted 8 January 2014; published online 23 January 2014)

Efficiency of the laser radiation energy transport into the shock wave generated in layered planar targets (consisting of massive Cu over coated by thin CH layer) was investigated. The targets were irradiated using two laser pulses. The 1ω pulse with the energy of ~ 50 J produced a pre-plasma, imitating the corona of the pre-compressed inertial confinement fusion target. The second main pulse used the 1ω or 3ω laser harmonics with the energy of ~ 200 J. The influence of the pre-plasma on parameters of the shock wave was determined from the crater volume measurements and from the electron density distribution measured by 3-frame interferometry. The experimental results show that the energy transport by fast electrons provides a definite contribution to the dynamics of the ablative process, to the shock wave generation, and to the ablation pressure in dependence on the target irradiation conditions. The strong influence of the pre-plasma on the investigated process was observed in the 1ω case. Theoretical analysis supports the explanation of experimental results. © 2014 AIP Publishing LLC. [<http://dx.doi.org/10.1063/1.4862784>]

I. INTRODUCTION

One of the main research aims related to the shock ignition concept (SI)^{1–3} is the investigation of the ablation pressure mechanism due to the laser spike at the intensity of $1\text{--}50$ PW/cm² and duration of several-hundred-ps, assuming that the main part of the absorbed laser energy is converted to fast electrons under the presence of the pre-plasma. The energy transfer by fast electrons into the plasma with supercritical density can provide an ablation pressure of several hundreds of Mbar, which is necessary for generating the igniting shock.^{4–6} Recent experiments with OMEGA laser^{7,8} seem to suggest an increasing efficiency of the energy transfer to both planar and spherical targets, resulting from the contribution of fast electrons generated due to stimulated Raman scattering and two-plasmon decay in an extended pre-plasma.

This work extends our previous research^{9–11} on the role of fast electrons in the laser energy conversion to shock waves performed with the PALS iodine laser, delivering a 300 ps duration pulse at intensities of $1\text{--}50$ PW/cm² using the first (1ω , 1314 nm) and third (3ω , 438 nm) harmonics radiation. In those experiments, massive targets of Al and Cu have been irradiated at various focal spot radii of the laser beam, R_L , to identify the mechanisms of laser absorption and to determine their influence on the absorbed energy transfer to the target. The mass of the ablated solid material as well

as the fraction of the laser energy deposited in the plasma have been determined by using the 3-frame interferometer and by measuring the volume of the crater created on the solid surface. Each of the interferometric channels is equipped with own independent interferometer system of the wave type.¹² Interferometer is irradiated by a part of the 1ω main beam subsequently converted to the second harmonic. Interferograms provided by these interferometers are obtained by separation, inversion, and folding of the front face of the probing wave.

The experiments have shown a strong influence of the wavelength and the intensity of the laser beam on the efficiency of the laser energy transfer to the massive target, independent from its material. 2D numerical simulations, including fast electrons transport^{10,13} as well as theoretical analysis based on an analytical model,¹¹ fully confirmed the experimental results and demonstrated conclusively that in the case of 1ω , intensities of $10\text{--}50$ PW/cm² and without pre-plasma on the target surface, the dominant ablation mechanism is heating by fast electrons generated at the resonant absorption. For the maximum laser energy of 580 J and intensity of 50 PW/cm², the ablative pressure reaches about 180 Mbar in spite of two-dimensional expansion of the target corona.^{9,10} However, for 3ω , the ablation pressure originates from the thermal electron conductivity heating, and its value of about 50 Mbar is several times lower in comparison with the 1ω case.^{9,10}

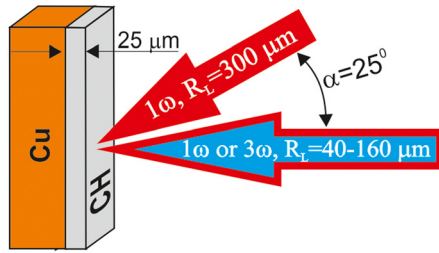


FIG. 1. Scheme of the layered target and its irradiation by laser beams.

The results of the next step experiment directed to the study of the pre-plasma effect on the ablation and the energy conversion efficiency to the shock wave are reported below.

II. EXPERIMENTAL CONDITIONS AND RESULTS

As shown in Fig. 1, this investigation used planar layered targets consisting of massive Cu and a 25- μm -thick layer of light plastic (CH) material. Accordingly to the SI concept, targets were irradiated using two laser pulses. The first 1ω beam with energy of $\sim 50\text{ J}$ produced a pre-plasma imitating the corona of the pre-compressed inertial confinement fusion (ICF) target that is a spherical target destined for creation an inertially confined thermonuclear plasma under an action of pulsed energy driver. The spike-driven shock wave was generated by the main pulse with energy of $\sim 200\text{ J}$ (either at 1ω or 3ω). The influence of the pre-plasma on the shock wave parameters was determined from measurements of the crater volume and the electron density distributions measured by 3-frame interferometry.

Interferograms were registered 2 ns after the second laser pulse maximum. This registration time seems to be optimum, since the processes of the absorption of the laser radiation in the plasma plume terminated already. The delay between the main and the auxiliary laser beams was kept fixed to $\Delta t = 1.2\text{ ns}$. Interferograms were registered for different focal spot radii R_L in the range of 40–160 μm . Typical interferograms obtained at 1ω or 3ω , with and without pre-plasma, are shown in Figs. 2 and 3.

In the case of the pre-plasma absence, Fig. 2, the raw interferograms display very high axial symmetry, both for 1ω and 3ω . In contrast, this symmetry is partially disturbed by the 1ω beam which produces the pre-plasma (see Fig. 3). The phase distribution results (calculated on the basis of the shifts of interference fringes) indicate that in the case of 1ω the axial asymmetry does not exceed 15% and slightly more only for 3ω . To solve the Abel equation, average values of the phase corresponding to the top and the bottom halves of the interferogram were taken into account. The FFT (Fast Fourier Transform)¹⁴ was applied for the electron density determinations. Because the inaccuracy of determination of the shifts of the fringes (the method of the *maximum fringe*¹⁵) is relatively high (several percent only), the accuracy of the electron density determination results from the degree of the axial symmetry of the investigated plasma. That is why outside of the opacity zone, in the case of no pre-plasma, the density error is small—at the level of 10%. For the pre-plasma case, it is somewhat larger but still does not exceed 30%.

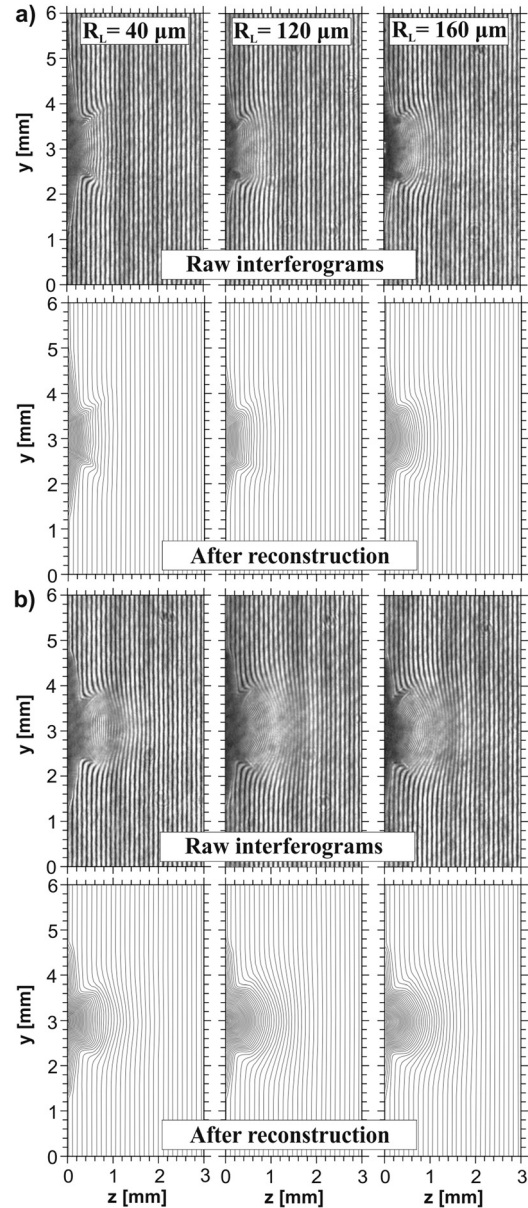


FIG. 2. Raw interferograms and their reconstructions for the case without pre-plasma and: (a) 1ω and (b) 3ω radiation.

An example of plasma density profile obtained from the interferograms is shown in Fig. 4.

The density profile on axis follows an exponential decay to a good approximation $n_e(z) = n_0 e^{-z/L}$. The parameters of this function determine the maximum electron density gradient in the opacity zone: $[dn_e/dz]_{z=0} = n_0/L$, where L is the scalelength of the density gradient and n_0 is the maximum electron density.

From the 2D density profile, one can calculate N_e , the total electron number in the plasma plume, assuming cylindrical symmetry. (A condition which is already applied in order to use Abel inversion for the determination of density from the interferogram.)

Another quantity, which was measured in the experiment, is the crater volume V_{cr} . In order to obtain information about the shape and dimensions of the craters, we used their replicas made of cellulose acetate (see Fig. 5).

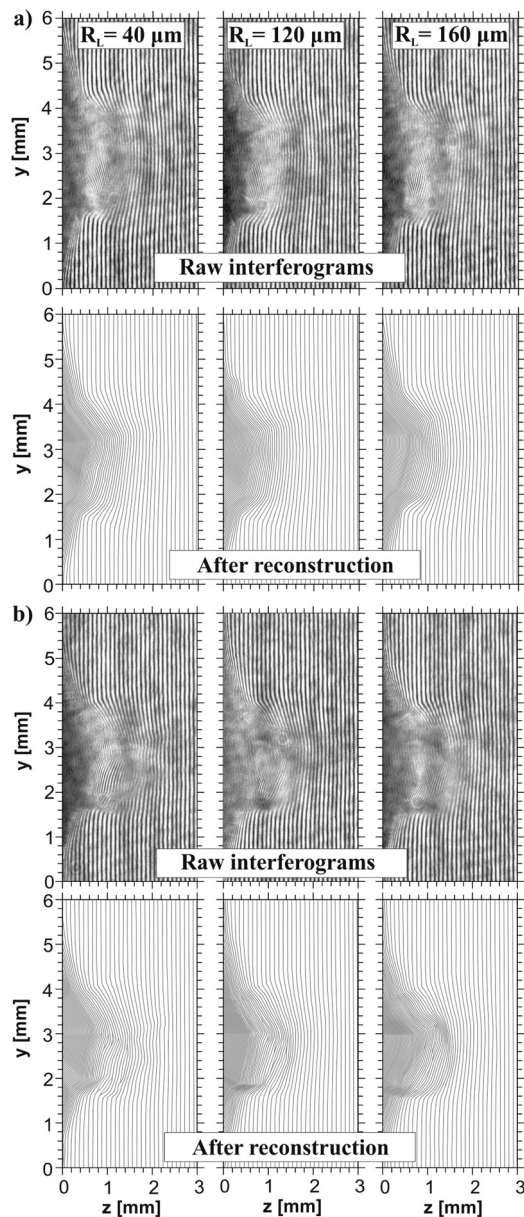


FIG. 3. Raw interferograms and their reconstructions for the case with pre-plasma and: (a) 1ω and (b) 3ω .

To reconstruct quantitatively the crater shape, microphotography was employed. The crater shape in a chosen cross-section was digitized to provide data for subsequent calculations. As some craters are not quite symmetrical and their shapes are irregular, photographs of their replica were made

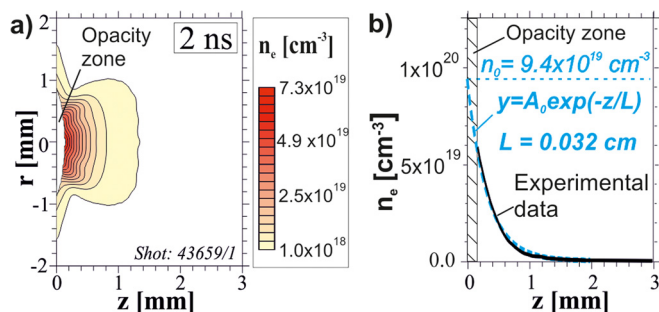


FIG. 4. Determination of the maximum electron density gradients: (a) experimentally obtained density distribution and (b) density profile on axis.

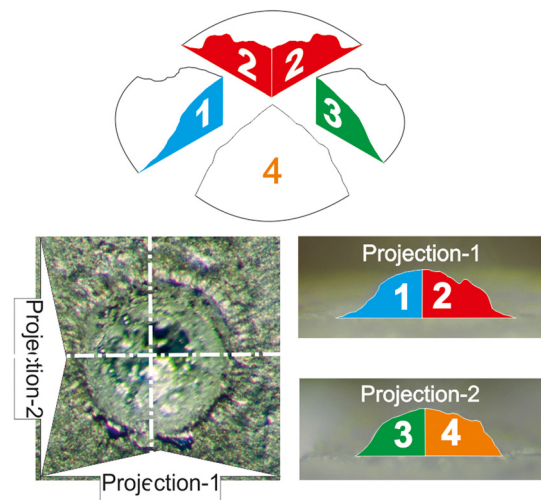


FIG. 5. Crater volume determination.

in two mutually perpendicular directions. Therefore, the volumes of the craters were determined by splitting them into quarters prior to calculations, as shown in Fig. 5. Each quarter of the crater volume was then evaluated independently. Finally, summation of these intermediate results provided the total crater volume.

Fig. 6 presents a comparison of the crater volumes V_{cr} and the N_e/V_{cr} ratios obtained for the two wavelengths (1ω and 3ω) without and with the pre-plasma (N_e is the total electron number in the plasma plume). The importance of N_e/V_{cr} parameter is described in Ref. 9.

Since the laser energy is constant ($E = 200$ J), by varying the focal spot radius, we also vary the laser intensity on target. Typically, when we vary the focal spot radius between 40 and 160 μm , the laser intensity changes between 1.6×10^{16} W/cm^2 and 1.0×10^{15} W/cm^2 . As shown in Fig. 6(a), without pre-plasma, the dependences of V_{cr} and N_e/V_{cr} on R_L are similar to both Al and Cu targets presented in Refs. 9 and 10. In the 3ω case with the predominant inverse bremsstrahlung absorption,¹¹ the efficiency of the crater creation

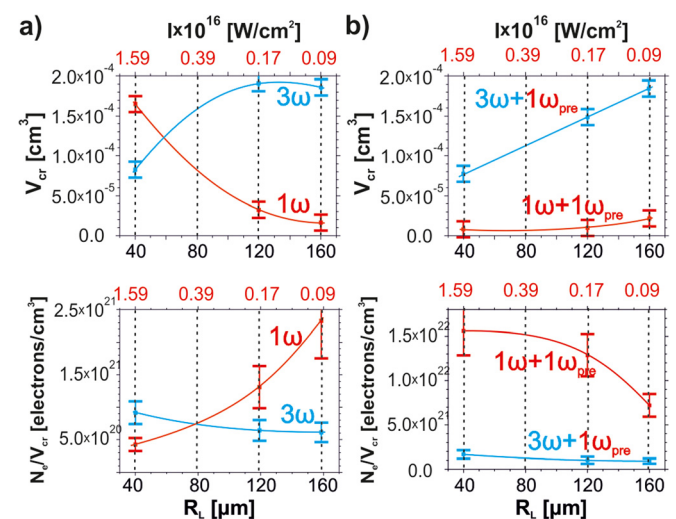


FIG. 6. Dependence of the crater volume and the N_e/V_{cr} ratio on the focal spot radius of the main laser beam in the case of (a) without and (b) with the pre-plasma. The data correspond to target presented in Fig. 1, laser energy $E = 200$ J, and delay $\Delta t = 1.2$ ns in all shots.

reduces with decreasing R_L due to the lateral expansion effect. In contrast, for 1ω , the efficiency of the crater creation increases with the decreasing R_L , which according to numerical simulations directly corresponds to the energy transfer to the target by fast electrons generated due to resonant absorption.

The strong influence of the pre-plasma on the crater creation process in the case of 1ω is clearly seen in Fig. 6(b). The crater volume decreases by more than one order of magnitude and simultaneously, N_e/V_{cr} increases by the same rate. It can be assumed that in the presence of pre-plasma the fast electron energy transfer effect becomes insignificant in 1ω case. In the case of 3ω , the pre-plasma influences the crater formation process only weakly, and both V_{cr} and N_e/V_{cr} values remain at the same level as in the case without pre-plasma. Under these conditions, the fast electron effect remains insignificant, in analogy to the case without pre-plasma.

The electron density distributions obtained for 1ω and 3ω in the cases with and without pre-plasma at different focal spot radii (R_L) are presented in Fig. 7. These data clearly demonstrate an effect of the pre-plasma on the main laser beam interaction with the target. Without the pre-plasma and in the 1ω case, Fig. 7(a), the plasma is more expanded in the radial direction and has a characteristic minimum on the z -axis.

This is clearly visible from the density distributions for $R_L = 40 \mu\text{m}$. In contrast with 1ω , for the case of 3ω , the plasma expansion is directed along the z -axis. Both the axial range and the axial density grow up with the increasing R_L . The presence of the pre-plasma, Fig. 7(b), results in limited radial expansion of the central plasma produced by the main beams (1ω and 3ω). In the case of 3ω , the radial limitation of the central plasma expansion part is larger, i.e., the expansion character is more axial.

The dependencies of the maximum density gradient, the maximum electron density, and the scalelength on R_L for the above-mentioned conditions of the target irradiation are shown in Fig. 8.

Without pre-plasma and using 1ω , Fig. 8(a), the density gradient increases strongly with the decreasing R_L even for the radii smaller than $80 \mu\text{m}$. Conversely, in the case of 3ω , the density gradient decreases with the decreasing focal spot radius. For $R_L < 80 \mu\text{m}$, the density gradient scalelength of the ablative plasma created by means of the 1ω beam is about $200 \mu\text{m}$, which is almost twice smaller in comparison with the plasma generated by 3ω .

Without pre-plasma, both the crater volume and the density gradient decrease with the decreasing beam radius at 3ω , and, conversely, increase (particularly strongly at the small radii of 40 and $80 \mu\text{m}$) at 1ω . As previously shown,^{9,10} the energy transfer by fast electrons is responsible for the growth of the crater volume with the decreasing beam radius (i.e., increasing laser intensity) in the 1ω case. Below, we demonstrate that the same effect gives rise to the observed dependence of the density gradient. The presence of the pre-plasma obviously leads to the minimum growth of these characteristics with the decreasing beam radius. This means that under the presence of the pre-plasma, the effect of the energy transfer by fast electrons is insignificant.

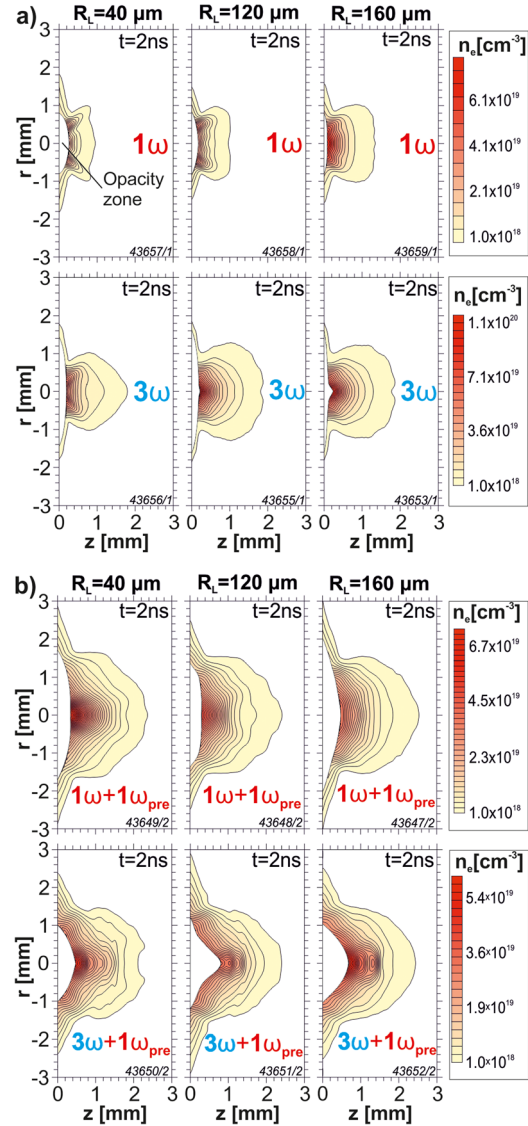


FIG. 7. Electron densities observed for the 1ω and 3ω radiation without (a) and with (b) the pre-plasma at different R_L .

III. DISCUSSION OF THE EXPERIMENTAL RESULTS

The essence of the energy transfer by fast electrons without pre-plasma can be explained by means of simple relations. The crater volume is determined by the fraction of the laser-produced plasma (plasma plume) energy E_p which is transmitted to the energy E_s of the shock wave propagating in the solid part of the target and creating the crater, $V_{cr} = K_p \sigma_p E_L / \alpha \varepsilon \rho$, where $K_p = E_p / E_L$ is the coupling efficiency, $\sigma_p = E_s / E_p$ is the ablation loading efficiency, ε is the specific energy required to vaporize a unit mass of the material, the parameter α^{-1} is the fraction of thermal energy corresponding to shock adiabat of the material, and ρ is density of solid material. In the approximation of the planar expansion, the energies E_p and E_s are determined by the values $P_a w_a$ and $P_s w_s$, respectively. Here, the pressure behind the shock wave P_s is close to the ablation pressure P_a (the pressure at the ablation front, i.e., at the border between the plasma plume and the target), and the velocities behind the ablation and shock wave fronts are w_a

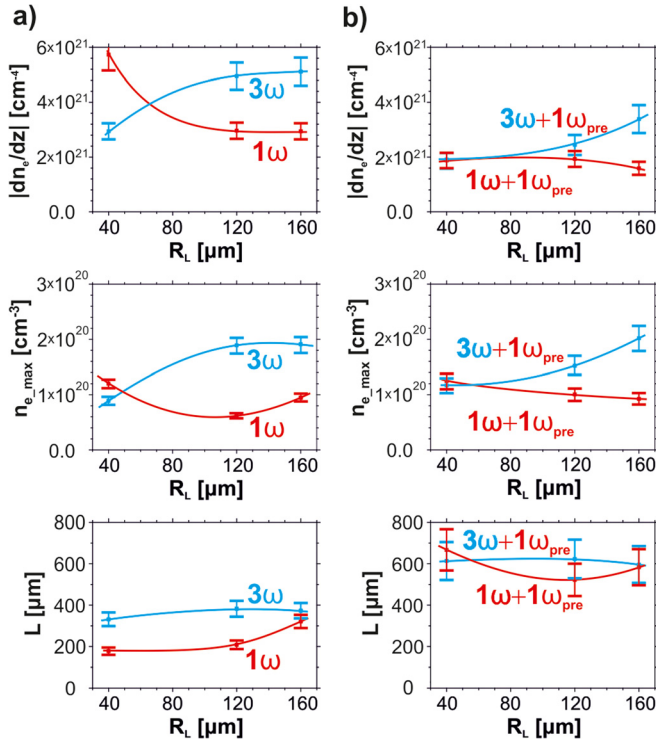


FIG. 8. Maximum density gradient for 1ω and 3ω without (a) and with (b) the pre-plasma.

$\propto (P_d/\rho_a)^{1/2}$ and $w_s \propto (P_s/\rho)^{1/2}$, respectively (ρ_a is the ablation density, i.e., the density at the ablation front). This is in agreement with the well-known result $\sigma_p \propto (\rho_a/\rho)^{1/2}$, see Ref. 16. The ablation density is uniquely expressed through the areal mass of the evaporated part of the target μ , $\rho_a \propto \mu/L_p$, where $L_p = (I\tau^3/\mu)^{1/2}$ is the size of the plasma plume, $I = K_p L$, and τ is the duration of the laser pulse. Therefore, $\rho_a \propto \mu^{3/2}/I^{1/2}\tau^{3/2}$. The analytical model of axially symmetric lateral plasma expansion due to the pulse ablation of the plane target by laser beam with a given radius R_L was developed in Ref. 11 on the basis of self-similar solution,¹⁷ describing the isothermal expansion of a portion of the material with a given mass. The model consists in a combination of self-similar solutions for the plane and spherical geometries in one solution, being a function of the parameter L_p/R_L . The expressions obtained for ρ_a and σ_p are

$$\rho_a = \frac{3}{(2\pi)^{1/2}} \frac{\mu^{3/2}}{I^{1/2}\tau^{3/2}} \Psi^{-2}, \quad (1)$$

$$\sigma_p = \frac{2^{1/2}\mu^{3/4}}{(2\pi)^{3/4}(\gamma+1)^{1/2}I^{1/4}\tau^{3/4}\rho^{1/2}} \frac{\Psi^{1/2}}{(2\Psi-1)^{3/2}}, \quad (2)$$

where the factor of the lateral expansion is defined by

$$\Psi = \left(1 + \frac{2^{3/4}L_p}{3R_L}\right)$$

and γ is the adiabatic index.

The areal evaporated mass μ is determined either by the depth of the matter heating by thermal conductivity wave during the period of laser pulse action

$$\mu_c \approx \kappa^{1/3} I^{2/3} \tau^{2/3} C_V^{-7/6} \quad (3)$$

or by the range of fast electrons^{10,11}

$$\mu_e = \frac{E_0^2 \cdot A \cdot m_p}{4\pi e^4 \cdot Z \cdot \Lambda}, \quad E_0(\text{keV}) \approx 8 \left(I_{L(pw)} \lambda_\mu^2 \right)^{2/3}. \quad (4)$$

Here, $\kappa(\text{erg} \times \text{cm}^{-1} \times \text{s}^{-1} \times \text{keV}^{-7/2}) = 8.4 \times 10^{19}/(Z+3.3)$ is electron conductivity coefficient (at the value of Coulomb logarithm $\Lambda = 5$, which was chosen as a scale for the ranges of plasma temperature and density of 0.5–2 keV and 0.05–0.2 g/cm³, respectively), $C_V = Zk_B/Am_p(\gamma-1)$ is the specific heat, Z and A are the charge and atomic number of the plasma ions, k_B is the Boltzmann constant, m_p is the proton mass, E_0 is the energy of fast electrons, e is the electron charge, and λ_μ is the laser radiation wave length measured in μm .

In the case of two-layer target, the scenario of crater creation in Cu-bulk is the following. Ablation pressure of the laser-produced plastic plasma excites and supports the shock wave in a solid plastic, during the period of the laser pulse. This shock wave propagates first in the relatively thin plastic layer and then in the Cu-bulk, where it produces a crater with the depth of several hundred μm (significantly larger than plastic layer thickness) during the period of several tens of ns (significantly longer than laser pulse). The main energy losses of the shock wave in thin plastic layer occur due to its reflection from the boundary between the plastic layer and the Cu-bulk. Under the approximation of strong wave, and assuming the density of plastic ρ_1 significantly smaller than the density of copper, ρ_2 the ratio of the energy of shock passing into Cu-bulk related to the energy of incident wave is well known to be $\sigma_s \approx [(\gamma_1+1)/(\gamma_2+1)]^{1/2}(\rho_1/\rho_2)^{1/2}$, where γ_1 and γ_2 are the adiabatic exponents of plastic and copper, respectively. So, the expression for the crater volume created in the Cu-bulk of the two-layer target is

$$V_{cr} = \frac{K_p \sigma_p \sigma_s E_L}{\alpha \varepsilon \rho_2}, \quad (5)$$

where $\sigma_s \approx 1/3$ under the neglecting its the weak dependence on γ_1 and γ_2 , and $\alpha \varepsilon \approx 2.3 \times 10^3 \text{ J/g}$ for copper.

Consequently, the dependence of the crater volume on the beam radius is determined by the ablation loading efficiency for the laser-produced plasma of the plastic ablator. Under conditions of the considered experiments, the expressions (3) and (4) show the following relationship between the ablated masses of plastic μ_c and μ_e . In the 3ω case, $\mu_c > \mu_e$ for all radii; in the 1ω case, $\mu_c > \mu_e$ for the radii $R_L = 160$ and $120 \mu\text{m}$ but $\mu_c < \mu_e$ for the radii $R_L = 80$ and $40 \mu\text{m}$. The energy transfer by fast electrons provides a stronger growth of the areal mass, and consequently a stronger growth of the ablation density of the flat layer with the increasing laser intensity than the thermal conductivity wave: $\rho_{a(e)} \propto I^{3/2}$, while $\rho_{a(c)} \propto I^{1/2}$. At a given laser intensity, this means that $\rho_{a(e)} \propto R_L^{-3}$, while $\rho_{a(c)} \propto R_L^{-1}$. At the beam radii of $R_L = 160$ and $120 \mu\text{m}$, for both harmonics, the ablation process is induced by the thermal conductivity wave and the lateral expansion effect is negligible, i.e., $L_p < R_L$. Therefore, $\rho \approx \rho_{a(c)}$ and V_{cr}

$\propto \sigma_{(c)} \propto R_L^{-1/2}$. Consequently, for large beam radii at both harmonics, the crater volume depends weakly on the radius. For small beam radii of $R_L = 80$ and $40 \mu\text{m}$, the lateral expansion effect is strong, $L_p \gg R_L$, and therefore, $\rho/\rho_a \propto (R_L/L)^2 \propto R_L^2 \mu/I$. From this, we get $\rho_{(e)}/\rho_{a(e)} \propto R_L^{4/3}$ and $\rho_{(c)}/\rho_{a(c)} \propto R_L^{8/3}$. As a result, for the 3ω case when the ablation is due to the thermal conductivity wave we have $V_{cr} \propto \sigma_{(c)} \propto R_L^{5/6}$. For the 1ω when the ablation is provided by the fast electron heating we have $V_{cr} \propto \sigma_{(e)} \propto R_L^{-5/6}$.

Let us evaluate, as an example, the crater characteristics in the case of large radii. The estimations based on (2) and (3) give for ablation loading efficiency the values of $\sigma_s \approx 2.4 \times 10^{-2}$ and $\sigma_s \approx 6.5 \times 10^{-2}$, respectively, for 1ω and 3ω cases. Substitution of these values as well as the values of $\sigma_s = 0.33$, $\alpha\varepsilon = 2.3 \times 10^3 \text{ J/g}$, $\rho = 8.9 \text{ g/cm}^3$, $E_L = 200 \text{ J}$ into expression (5) gives the best agreement with experimental results at coupling efficiencies of $K_p = 0.2$ and $K_p = 0.6$ in the 1ω and 3ω cases, which correspond to calculated values of the crater volume $V_{cr} \approx 2 \times 10^{-5} \text{ cm}^3$ and $V_{cr} \approx 1.5 \times 10^{-4} \text{ cm}^3$, respectively. Under laser interaction with low-Z material, such as plastic, the energy losses due to thermal radiation are small and coupling efficiency is close to the absorption coefficient. The absorption coefficient of 0.2 in the 1ω case and 0.6 in the 3ω case is in a good agreement with numerical simulations of PALS laser interaction with low-Z material using the 2D ATLANT-HE code.^{9,10} For example, the volume $V_{cr} \approx 1.5 \times 10^{-4} \text{ cm}^3$ of semi-spherical crater corresponds to the crater radius equal, approximately, to $300 \mu\text{m}$. In this case, the evaluation of the average shock wave velocity for 3ω irradiation gives the value of $3 \times 10^5 \text{ cm/s}$ and the period of the crater creation is about 100 ns. Note that the crater scaling relations in the 3ω case give results close to observed ones in the all radii range. The crater scaling relations in the 1ω case give results close to observed ones at the large radii of 120 and $160 \mu\text{m}$ only. For small radii, the scaling relations give values of the crater volume smaller than observed ones. The reason for this consists in the fact that a fraction of fast electrons of high energy tail produces the crater by the direct heating of solid that is more efficient than the crater production by the shock wave.

Thus, in the 1ω case, the effect of the energy transfer in the dense plasma by fast electrons whose energy increases with the decreasing radius of the laser beam (with the increasing intensity) is stronger than the effect of the lateral expansion, whereby the efficiency of the energy transmission to the shock wave and also the crater volume increase with the decreasing beam radius. In the 3ω case, the effect of the thermal conductivity heating is weaker than the effect of the lateral expansion. Consequently, the efficiency of the energy transmission to the shock wave and the crater volume decrease with the decreasing radius of the beam.

The dependencies of the density gradient on the beam radius at different harmonics are also determined by the peculiarities of the ablation density formation at different mechanisms of the energy transfer by fast electrons and the thermal conductivity wave. Bearing in mind that after the laser pulse termination the plasma plume expands adiabatically, the density gradient at the time of the interferometry measurement t_i can be defined as

$$G \equiv \frac{dn}{dz} \approx C \frac{Z_q}{Am_p} \frac{\rho L_p}{L_i L_i}, \quad (6)$$

where the density ρ is given by (1), $L_i \approx t_i L_p / \tau$ is the size of the plasma plume in the time t_i , Z_q is the charge of the ions taking into account the quenching effect, and C is a constant. At large radii, $G \propto K_p^{1/3} R_L^{-2/3}$ for both harmonics. At small radii, $G \propto R_L^2$ for thermal conductivity (the 3ω case) and $G \propto K_p^{-1} R_L^{-2}$ for the energy transfer by fast electrons (1ω case). Theoretical dependencies of the density gradient calculated by the formulas (6), (3), and (4) for time $t_i = 3.45 \text{ ns}$ ($t_i = 14\tau$) are compared to the experimental values in the case without pre-plasma in Fig. 9.

The value $Z_q/A = 0.4$ was used on the basis of the quenching effect estimates for time $t_i = 3.45 \text{ ns}$, the values of the coupling efficiency K_p were 0.2 and 0.6 for 1ω and 3ω cases, i.e., the same as in above mentioned estimates. The best fit to the experimental data is provided by the constant $C = 1.8$.

A few comments should be added concerning the relevance of our results for the shock ignition approach to ICF. Of course, the described experiments are quite far from «realistic» ICF conditions. Nevertheless, we notice that simulations¹⁸ predict that for Laser Megajoule conditions, the distance between the ablation front (identified by the foot of the electron temperature profile), the critical density n_c occurs around $L_1 \approx 150 \mu\text{m}$ and the distance between n_c and $n_c/4$ is $L_2 \approx 350 \mu\text{m}$. These values are indeed comparable to results shown at the bottom of Fig. 8(b), although the pre-plasma is much colder due to the limited energy available for its creation.

Again, in connection to the relevance of these results to ICF, we should comment on impact of parametric instabilities in our experimental conditions. Indeed, such instabilities (stimulated Raman scattering (SRS), stimulated Brillouin scattering (SBS), and TPD) can, in principle, relate to a considerable amount of energy and therefore strongly affect the laser-target coupling conditions. In principle, the laser pulse duration of 300 ps used in PALS experiments is compatible with the well-developed parametric instabilities. Therefore, in order to provide a realistic estimate of the laser energy deposited on the target, accurate backscattering measurements are highly desired (see Refs. 19 and 20). On the other hand, we have measured SRS and TPD spectra as well as the total energy reflected within the lens cone due to SBS and SRS. In the same time, the energy reflected outside the lens cone has been estimated by using a few microcalorimeters placed inside the interaction chamber. The overall conclusion of the measurement is that in our

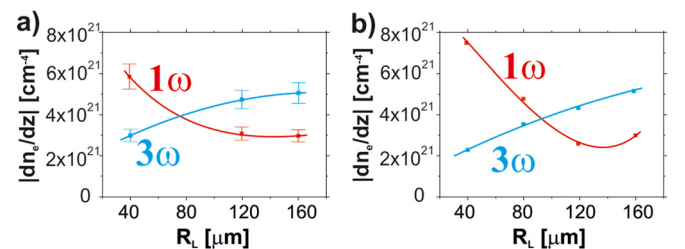


FIG. 9. Comparison of the maximum electron density gradients for both harmonics in the case without pre-plasma: (a) experimental and (b) theoretical data.

experimental situation, the fraction of incident laser light reflected due to parametric instabilities is always less than 10%.

Therefore, we can conclude that in our case the laser coupling efficiency on target is not deteriorated due to parametric instabilities.

IV. CONCLUSIONS

Two-beam experiments directed to imitate the spike-laser interaction with the pre-produced plasma have shown the significantly decreasing efficiency of the 1ω radiation energy transmission to the solid part of the target in comparison with the case without pre-plasma. Experiments with the single 1ω beam demonstrated an enhanced efficiency of energy transfer to shock wave associated with the fast electrons energy transfer to the dense plasma region.

The presence of the pre-plasma creates poor conditions for resonant absorption and, therefore, for the laser energy conversion to fast electrons. This results in suppression of the fast electrons contribution to the ablation process. The significantly smaller effectiveness of the energy transfer to dense plasma regions under the pre-plasma created by the high-intensity 1ω pulse is clearly seen from both the craters volumes and the density gradient data. On the other hand, two-beam experiments have not provided data indicating alteration of the fast electrons generation due to resonant absorption by any other mechanism connected with parametric plasma instabilities in the pre-plasma.

ACKNOWLEDGMENTS

This work was supported in part by the Access to Research Infrastructure activity in the 7th Framework Program of the EU Contract No. 284464, Laserlab Europe III, by the Czech Republic's Ministry of Education, Youth and Sports under PALS RI project (No. LM2010014), by National Centre for Science (NCN), Poland under Grant No. 2012/04/M/ST2/00452 and within the HiPER project under Grant Agreement No. 211737. The participation of S. Yu. Gus'kov and N. N. Demchenko in this work was supported by RFBF projects Nos. 14-02-00010 and 13-02-00295. The participation of O. Renner was supported by the Czech Science Foundation project No. CZ.1.07/2.3.00/20.0279 and by the ELI Project No. CZ.1.05/1.1.00/02.0061.

¹V. A. Scherbakov, "On the expediency of making double-pulse lasers for laser thermonuclear fusion," *Sov. J. Plasma Phys.* **9**, 240 (1983).

²R. Betti, C. D. Zhou, K. S. Anderson, L. J. Perkins, W. Theobald, and A. A. Solodov, *Phys. Rev. Lett.* **98**, 155001 (2007).

³L. J. Perkins, R. Betti, K. N. LaFortune, and W. H. Williams, "Shock ignition: A new approach to high gain inertial confinement fusion on the National Ignition Facility," *Phys. Rev. Lett.* **103**, 045004 (2009).

⁴S. Yu. Gus'kov, V. V. Zverev, and V. B. Rozanov, "Steady-state model of the corona of spherical laser targets allowing for energy transfer by fast electrons," *Sov. J. Quantum Electron.* **13**, 498 (1983).

⁵S. Yu. Gus'kov, X. Ribeyre, M. Touati, J. L. Feugeas, Ph. Nicolai, and V. Tikhonchuk, "Ablation pressure driven by an energetic electron beam in a dense plasma," *Phys. Rev. Lett.* **109**, 255004 (2012).

⁶L. Antonelli, D. Batani, A. Patria, O. Ciricosta, C. A. Cecchetti, P. Koester, L. Labate, A. Giulietti, L. A. Gizzi, A. Moretti, M. Richetta, L. Giuffrida, L. Torrisi, T. O'Dell, M. Kozlová, J. Nejd, M. Sawicka, D. Margarone, B. Rus, G. Schurtz, X. Ribeyre, M. Lafon, and C. Spindloe, "Laser-plasma coupling in the shock-ignition intensity regime," *Acta Tech.* **56**, T57 (2011).

⁷W. Theobald, R. Betti, C. Stoeckl, K. S. Anderson, J. A. Delettrez, V. Yu. Glebov, V. N. Goncharov, F. J. Marshall, D. N. Maywar, R. L. McCrory, D. D. Meyerhofer, P. B. Radha, T. C. Sangster, W. Seka, O. V. Shvarts, V. A. Smalyuk, A. A. Solodov, B. Yaakobi, C. D. Zhou, J. A. Frenje, C. K. Li, F. H. Séguin, R. D. Petrasso, and L. J. Perkins, *Phys. Plasmas* **15**, 056306 (2008).

⁸W. Theobald, R. Nora, M. Lafon, A. Casner, X. Ribeyre, K. S. Anderson, R. Betti, J. A. Delettrez, J. A. Frenje, V. Yu. Glebov, O. V. Gotchev, M. Hohenberger, S. X. Hu, F. J. Marshall, D. D. Meyerhofer, T. C. Sangster, G. Schurtz, W. Seka, V. A. Smalyuk, C. Stoeckl, and B. Yaakobi, *Phys. Plasmas* **19**, 102706 (2012).

⁹Z. Kalinowska, A. Kasperczuk, T. Pisarczyk, T. Chodukowski, S. Yu. Gus'kov, N. N. Demchenko, J. Ullschmied, E. Krousky, M. Pfeifer, J. Skala, and P. Pisarczyk, "Investigations of mechanisms of laser radiation absorption at PALS," *Nukleonika* **57**, 227 (2012).

¹⁰S. Yu. Gus'kov, N. N. Demchenko, A. Kasperczuk, T. Pisarczyk, Z. Kalinowska, T. Chodukowski, O. Renner, M. Smid, E. Krousky, M. Pfeifer, J. Skala, J. Ullschmied, and P. Pisarczyk, "Laser-driven ablation through fast electrons in PALS-experiment at the laser radiation intensity of 1–50 PW/cm²," *Laser Part. Beams* (published online).

¹¹S. Yu. Gus'kov, S. Borodziuk, M. Kalal, A. Kasperczuk, B. Kralikova, E. Krousky, J. Limpouch, K. Masek, P. Pisarczyk, T. Pisarczyk, M. Pfeifer, K. Rohlena, J. Skala, and J. Ullschmied, *Quantum Electron.* **34**(11), 989 (2004).

¹²S. Borodziuk, A. Kasperczuk, T. Pisarczyk, S. Yu. Gus'kov, J. Ullschmied, B. Kralikova, K. Rohlena, J. Skala, M. Kalal, and P. Pisarczyk, "Investigation of plasma ablation and crater formation processes in the Prague Asterix Laser System laser facility," *Opt. Appl.* **34**(1), 31 (2004).

¹³R. Liska, J. Limpouch, M. Kucharik, and O. Renner, "Selected laser plasma simulations by ALE method," *J. Phys.: Conf. Ser.* **112**, 022009 (2008).

¹⁴M. Kalal and K. A. Nugent, "Abel inversion using fast Fourier transforms," *Appl. Opt.* **27**(10), 1956 (1988).

¹⁵A. Kasperczuk and T. Pisarczyk, "Application of automated interferometric system for investigation of the behaviour of a laser-produced plasma in strong external magnetic fields," *Opt. Appl.* **31**(3), 571–597 (2001).

¹⁶S. Yu. Gus'kov, "Efficiency of hydrodynamic energy transfer to an arbitrarily thick flat layer of material during pulsed ablation," *J. Exp. Theor. Phys.* **97**, 1137 (2003).

¹⁷V. S. Imshennik, "The isothermal scattering of a gas cloud," *Sov. Phys. Dokl.* **5**, 263 (1960).

¹⁸E. Le Bel, G. Schurtz, X. Ribeyre, and M. Lafon, Shock Ignition Workshop: "1D PDD shock ignition design for NIF/LMJ," March 2011.

¹⁹P. Koester, L. Antonelli, S. Atzeni, J. Badziak, F. Baffigi, D. Batani, C. A. Cecchetti, T. Chodukowski, F. Consoli, G. Cristoforetti, R. De Angelis, G. Folpini, L. A. Gizzi, Z. Kalinowska, E. Krousky, M. Kucharik, L. Labate, T. Levato, R. Liska, G. Malka, Y. Maheut, A. Marocchino, T. O'Dell, P. Parys, T. Pisarczyk, P. Raczka, O. Renner, Y. J. Rhee, X. Ribeyre, M. Richetta, M. Rosinski, L. Ryc, J. Skala, A. Schiavi, G. Schurtz, M. Smid, C. Spindloe, J. Ullschmied, J. Wolowski, and A. Zaras, "Recent results from experimental studies on laser-plasma coupling in a shock ignition relevant regime," *Plasma Phys. Controlled Fusion* **55**, 124045 (2013).

²⁰C. A. Cecchetti, A. Giulietti, P. Koester, L. Labate, T. Levato, L. A. Gizzi, L. Antonelli, A. Patria, D. Batani, M. Kozlová, D. Margarone, J. Nejd, B. Rus, M. Sawicka, M. Lafon, X. Ribeyre, and G. Schurtz, "Parametric instabilities study in a shock ignition relevant regime," *Proc. SPIE* **8080**, 80802A (2011).